Fabrication and Study of the Magnetic Properties of $(Fe_{30}Co_{70})_{100-x}Zn_x$ Nanowire Arrays

A. Sedghi[a,*], F. Zolfi[b] and S. Vali Aghaie[c]

[a]Department of Physics, Shabestar Branch, Islamic Azad University, Shabestar, Iran

[b]bDepartment of Physics, University of Kurdistan, Sanandaj, Iran

[c]Sama technical and vocational training college, Islamic Azad University, Sanandaj Branch, Sanandaj, Iran

(Received April 19, 2014; revised version December 31, 2014; in final form February 21, 2015)

$(Fe_{30}Co_{70})_{100-x}Zn_x$ ($0 \leq x \leq 10$) nanowires with diameters of ≈37 nm have been fabricated by AC electrodeposition into pores of anodized aluminum oxide (AAO) templates. The $Fe_{30}Co_{70}$ and Zn contents of the nanowires have been adjusted by varying the ratio of $Fe_{30}Co_{70}$ and Zn ion concentrations in the electrolyte. The effect of the Zn content and annealing on the magnetic properties (e.g., coercivity and squareness) of nanowires arrays have been investigated using X-ray diffraction, scanning electron microscopy, and alternating gradient force magnetometer. X-ray diffraction patterns reveal that an increase in the concentration of Zn ions of the electrolyte results in significant reduction in coercivity and squareness. It was found that the magnetic properties of nanowires can be significantly improved by appropriate annealing process. The highest values for coercivity (2670 Oe) and squareness (0.99) have been obtained for nanowires electrodeposited using 95/5 and 98/2 $Fe_{30}Co_{70}$:Zn concentrations at annealing temperatures of 575 °C and 550 °C, respectively.

DOI: 10.12693/APhysPolA.127.1706

PACS: 81.07.Gf, 81.15.Pq, 75.75.–c

1. Introduction

In the past few years, the fabrication of nanowire (NW) arrays has attracted a lot of interest [1–4] due to their potential applications in high-density storage media [5], highly sensitive giant magnetoresistance (GMR) materials [6], sensors [7], biosensors [8], photocatalysts [9], thermoelectric cooling systems [10], and photonic crystals [11]. NWs have been fabricated using different methods such as chemical vapor deposition [12], electroless growth [13], and electrodeposition [14]. The electrodeposition technique has revealed itself to be an easy method of controlling compositions of NWs [15] and both length and diameter of pores [16]. Among different electrodeposition methods, template-assisted techniques appear to be promising due to simplicity and the high level of control over the morphology, microstructural properties, packing density, size and physical properties of NWs by tuning the template and electrodeposition parameters. In comparison to DC methods, AC electrodeposition requires a less complex sample preparation process and leads to higher filling factor, which is very important for practical applications. Also among other templates, anodized aluminum oxide (AAO) templates have been more widely used to prepare NWs because the diameter, center to center spacing between the holes and lengths of the holes can be controlled by changing anodizing conditions and subsequent procedure. Furthermore, AAO template is stable at higher temperature, which opens up the possibility of studying how annealing affects the structure and properties of NWs. Many attempts have been focused on the fabrication of NW alloys in order to improve the magnetic and mechanical of the NWs for practical application and to study performances the fundamental mechanisms behind the magnetic properties of these materials. For the case of FeCo, different NW alloys such as FeCo [17–19], FeCoTb [20], FeCoP [21–23], FeCoSi [24, 25], FeCoPb [26] and FeCoNi [27] have been reported. In this work, we have fabricated and investigated the magnetic properties of FeCoZn NW alloys. The effect of Zn concentration and annealing on the coercivity (Hc) and squareness (Sq) of FeCoZn NWs is investigated.

2. Experimental procedure

FeCoZn NW arrays have been fabricated using electrodeposition and template method. AAO was made by anodizing the aluminum foils in a conventional two-step process [15]. Discs with 8 mm in diameter and 0.3 mm thick of high purity (99.999%) aluminum were ultrasonically degreased in acetone followed by annealing at 450 °C for 1 h in high purity Ar. Samples were then etched in 3 M NaOH at room temperature for about 3 min for removing the oxide layer prior to an anodization process. Samples were then washed and electropolished in 1:4 (v/v) solutions of perchloric acid and ethanol at 25 °C. Conventional two-step mild anodization process was employed to obtain highly ordered with high aspect ratio pores. The first anodization was carried out in 0.3 M oxalic acid electrolyte at 40 V and 17 °C for 15 h with 23 mm distance between anode and cathode. The anodized layer was then removed by immersing the samples to a solution containing 0.2 M chromic acid and 0.5 M phosphoric acid 15 h at 70 °C. The second anodization was carried out at the same conditions for 1 h. The thickness

*corresponding author; e-mail: aliasgharsedghi@gmail.com

of barrier layer was estimated to be about 40 nm since barrier layer thickness had been reported to be about 1 nm V^{-1} [28]. This barrier layer is too thick for electrodeposition process due to its high resistivity, and thus needs to be thinned.

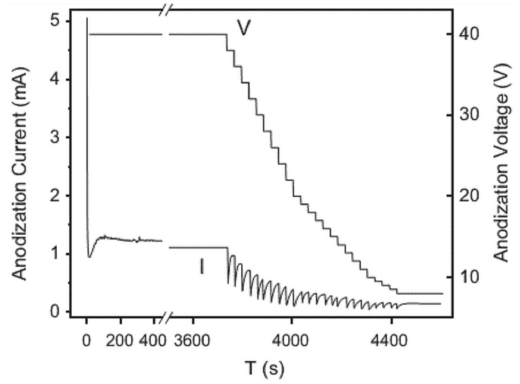

Fig. 1. A typical anodization current and voltage during the second anodization and barrier layer thinning process.

The thinning process was performed by decreasing the anodization voltage in three stages as shown in Fig. 1. In the first stage, the anodization voltage was decreased by 2 V min^{-1} from 40 V to 20 V. The anodization voltage then decreased from 20 V to 10 V in the rate of 1 V min^{-1} followed by decreasing to 8 V with the rate of 0.5 V min^{-1}. At the end, the anodization process was continued for 3 min at 8 V in order to obtain uniform barrier layer. The final thickness for barrier layer was estimated to be about 8 nm. In summary, on the surface of aluminium an oxide layer of 2–5 nm thickness is composed in the presence of H_2O and O_2. Porous oxide layer is obtained by the use of oxalic acid and applying the certain voltage. Electrode is composed of platinum or graphite as the cathode and aluminium as the anode. Pores grow perpendicular to the surface of aluminium and when the aluminum is anodized in acidic solutions, pores in a exactly hexagonal order were formed (Fig. 2).

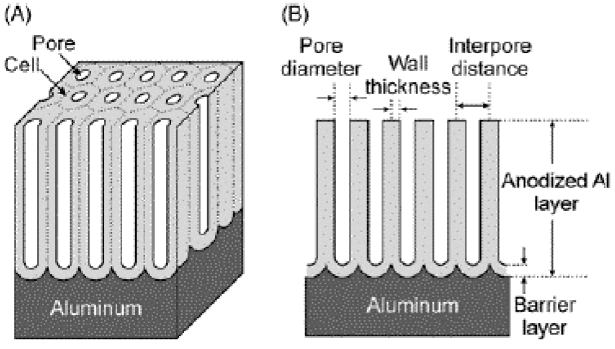

Fig. 2. Hexagonal array of porous Al_2O_3 film prepared by anodization of Al in oxalic acid.

According to the experimental results, the highly ordered porous structure on the aluminium template is formed at 40 V. FeCoZn NW alloys were then prepared by co-electrodeposition of Fe^{+2}, Co^{+2} and Zn^{+2} ions in the AAO pores at room temperature. AC sine wave (30 V_{pp}) was used for electrodeposition. A solution of $(100-x)FeSO_4{\cdot}7H_2O$ (83.4−75.06 g/l), $(100-x)CoSO_4{\cdot}7H_2O$ (196.77−177.09 g/l), $xZnSO_4{\cdot}7H_2O$ (0−28.75 g/l), 3 g/l boric acid and 1.5 g/l ascorbic acid was used as the electrolyte. At the beginning the pH value of the electrolyte was about 3.2, but it was adjusted to 4 and maintained constant during the experiment with NaOH. The electrolyte was continuously agitated during the deposition procedure. The Zn content of the NWs has been adjusted by varying x and the effect of different annealing temperatures on magnetic properties has been discussed. Morphology of samples has been studied by scanning electron microscope (SEM) and transmission electron microscope (TEM). Magnetic properties of the NWs embedded in the AAO templates have been measured by an alternating gradient force magnetometer (AGFM). The crystal structure and composition of NWs have been characterized by X-ray diffraction (XRD) and electron diffraction (EDX), respectively.

3. Results and discussion

Figure 3a shows a typical top view SEM micrograph of a pore structure after the second anodization process. As it can be seen, pores are well distributed in the hexagonal pattern, which is an ideal pattern for anodized AAO. The average pore diameter and spacing are about 37 nm and 70 nm, respectively. A typical cross-sectional SEM micrograph of AAO pore structure is displayed in Fig. 3b, which displays high aspect ratio parallel cylindrical nanopores without intercrossing. Figure 3c shows the TEM image of the FeCoZn NWs released from the AAO template. To release the

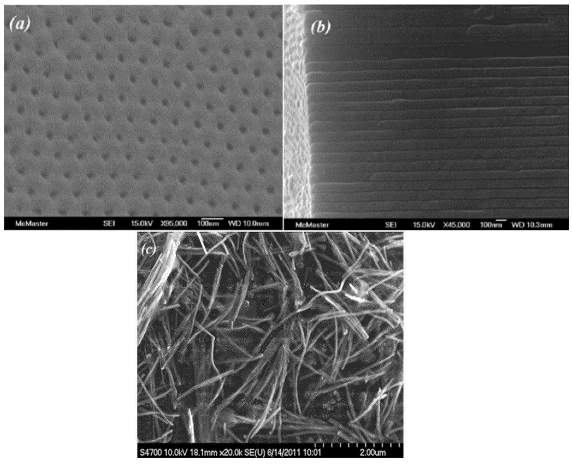

Fig. 3. A typical (a) top and (b) cross-sectional view SEM micrograph of AAO pore structure after the second anodization. (c) TEM image of the NWs released from the AAO template.

NWs from the AAO templates the electrodeposited mem-

branes have been dissolved in the solution containing 0.2 M chromic acid and 0.5 M phosphoric acid. NWs were then washed several times by distilled water and dispersed in methanol. The diameter of as-synthesized NWs is almost the same as AAO pore diameter. The sharp contrast along the NWs shows polycrystalline properties of NWs. The length of NWs varies from 1 μm up to 2 μm depending on the electrodeposition time. Therefore, NWs have an aspect ratio (length to diameter) ranging from 30 to 60. The quantitative EDX analysis reveals that Fe, Co and Zn content of as deposited NWs depends on the ionic concentrations of Fe^{+2}, Co^{+2} and Zn^{+2} in the electrolyte. Six groups of samples have been prepared using the solution of $(100-x)FeSO_4 \cdot 7H_2O$ (83.4–75.06 g/l), $(100-x)CoSO_4 \cdot 7H_2O$ (196.77–177.09 g/l), $xZnSO_4 \cdot 7H_2O$ (0–28.75 g/l) with x = 0, 1, 2, 5, 7.5, and 10 as electrolyte. Samples have been AC electrodeposited by a sine wave, V_{pp} = 30 V and f = 200 Hz. The pH of the electrolyte has been adjusted to 4 and maintained constant during the procedure at room temperature.

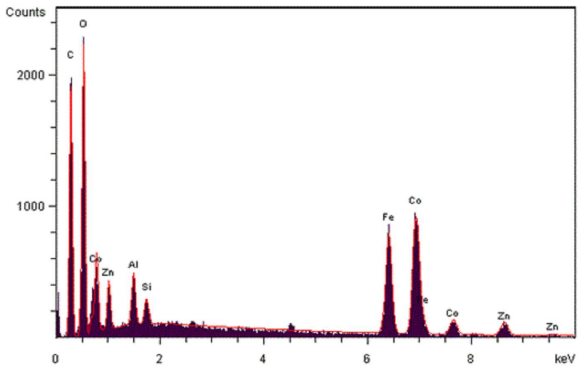

Fig. 4. A typical EDX result of NW arrays.

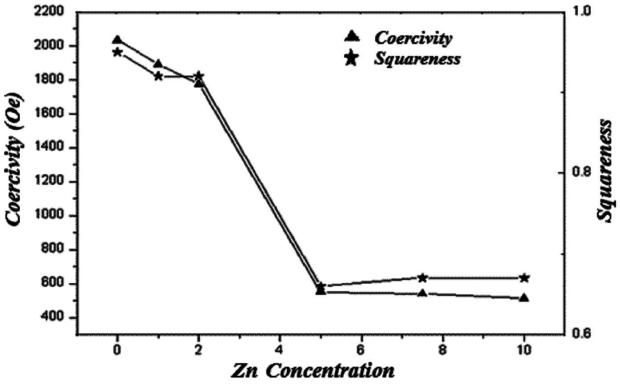

Fig. 5. The variation of Hc and Sq of the $(Fe_{30}Co_{70})_{100-x}Zn_x$ of NW arrays (for x = 0, 1, 2, 5, 7.5 and 10) versus Zn content.

A typical EDX electrodeposition result of NW arrays is shown in Fig. 4, displaying the presence of Fe, Co and Zn in the NWs. Because of interesting magnetic properties, we have concentrated on the $Fe_{30}Co_{70}$ NWs [18] and the effect of the Zn content on the magnetic properties of $(Fe_{30}Co_{70})_{100-x}Zn_x$ (x = 0, 1, 2, 5, 7.5, 10) NW alloys has been investigated before annealing process. The variation of coercivity (Hc) and squareness (Sq) of these NW arrays versus the Zn content is shown in Fig. 5.

Both Hc and Sq decrease by increasing the nonmagnetic Zn content of the NWs. The Hc and Sq significantly decrease from 2032 Oe and 0.95 for $Fe_{30}Co_{70}$ (x = 0) sample to about 560 Oe and 0.66 for $(Fe_{30}Co_{70})_{90}Zn_{10}$ (x = 10) sample, respectively. It is known that the Hc depends on the magnetization reversal process. The magnetization process of NWs can be explained by a model consisting of a chain of spheres with symmetric fanning, where each NW is considered as an ideal chain with N single-domain spheres [29].

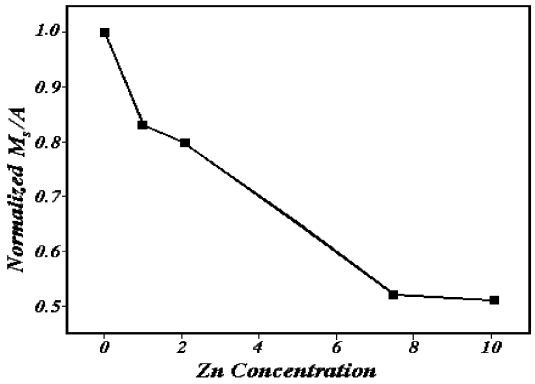

Fig. 6. The variation of saturation magnetization per area unit of NW versus the Zn content.

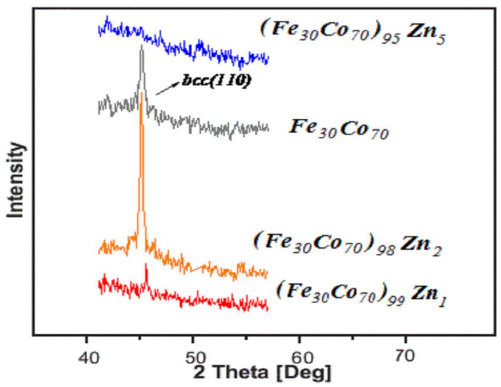

Fig. 7. The XRD patterns of the $(Fe_{30}Co_{70})_{100-x}Zn_x$ NW arrays.

According to this model, the Hc is directly proportional to the saturation magnetization (Ms), which increases with N and remains constant for $N > 10$. The reduction in Hc value of as prepared NW arrays can be explained since the Ms of $(Fe_{30}Co_{70})_{100-x}Zn_x$ NW arrays decreases with increase of the Zn content. The variation of Ms/A (A is the area of the sample) versus the Zn content is shown in Fig. 6. To further investigation of the effect of the Zn content on the structural properties of NWs, the crystal structure of the samples has been studied. The XRD patterns of the NW arrays are shown

in Fig. 7. The height of nanowire is not very important in this figure. The peak in the nanowire with 2% Zn is higher than other nanowires and this shows that without Zn, the nanowire structure is bcc and Zn makes it highly ordered. As it can be seen, the as deposited $Fe_{30}Co_{70}$ ($x = 0$) NWs has bcc structure with (1 1 0) axis, indicating that the NWs axis is along this axis. The intensity of the peaks for $(Fe_{30}Co_{70})_{99}Zn_1$ ($x = 1$) NW sample is lower, indicating that the crystallinity decreases due to the presence of Zn. The intensity of the peaks increases for $(Fe_{30}Co_{70})_{99}Zn_1$ ($x = 2$) NWs because the atomic radius of Zn is larger than it for Fe and Co and it makes the height of Nws larger and then the Hc increases. By further increasing the Zn content, the peaks disappear for $(Fe_{30}Co_{70})_{95}Zn_5$ ($x = 5$) sample, revealing an amorphous phase for the NW.

By increasing the Zn content, all samples remain in the amorphous phase. Based on these results, it is obvious that crystal structure of the arrays of $(Fe_{30}Co_{70})_{100-x}Zn_x$ ($x \geq 5$) NW alloys gradually change from bcc crystalline phase to amorphous phase with an increasing Zn content, which is in agreement with recent reports [30]. Further increase in the Zn content significantly reduces the Ms of the NW arrays, resulting in a strong deterioration in both Hc and Sq. It has been shown that proper annealing process can improve the magnetic properties of NWs [17, 31]. Here, the effects of annealing temperature on the magnetic properties of NW alloys have been investigated in order to obtain the optimum magnetic properties for NW arrays. Samples were annealed at different temperatures, ranging from 200 °C to 600 °C, in a 90% Ar and 10% H atmosphere for 30 min followed by slow cooling to room temperature.

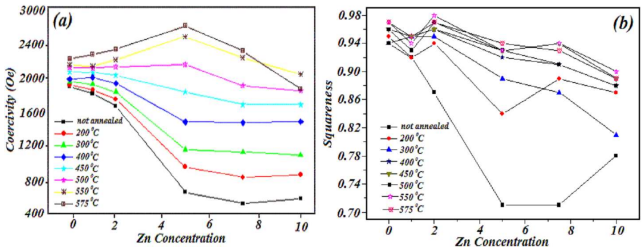

Fig. 8. The effect of annealing temperature on the (a) Hc and (b) Sq values of NW arrays for different Zn concentrations.

Figure 8 illustrates the effect of annealing temperature on the Hc and Sq values of the NW arrays. As it can be seen, Hc and Sq of all samples increase with annealing at all annealing temperatures up to 575 °C. In particular, the Hc and Sq values of the $(Fe_{30}Co_{70})_{95}Zn_5$ sample increase from 550 Oe and 0.66 for as deposited sample to 2670 Oe and 0.89 after annealing at 575 °C, respectively. The maximum value of Sq is 0.99 for $(Fe_{30}Co_{70})_{98}Zn_2$ sample at 550 °C. The magnetic properties of the samples deteriorated by increasing the annealing temperature further to 600 °C (not shown in this figure) due to the distortion of the aluminum substrate and AAO membrane.

Figure 9 shows typical hysteresis loops of $(Fe_{30}Co_{70})_{95}Zn_5$ NW sample for external magnetic field parallel to the NW before and after annealing. The hysteresis loop has a square shape after annealing and a narrow loop before annealing, indicating that Sq value increases by annealing.

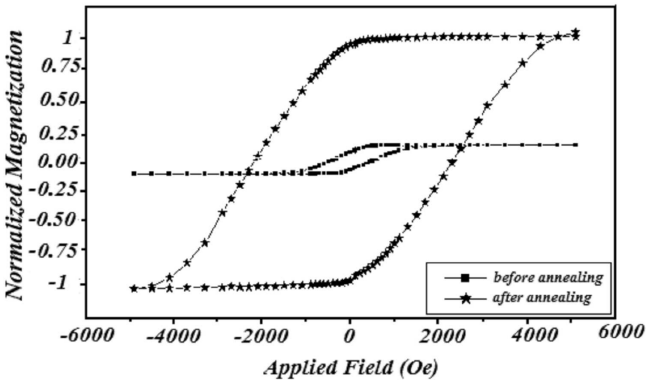

Fig. 9. The hysteresis loops of $(Fe_{30}Co_{70})_{95}Zn_5$ NW arrays for the case of external magnetic field parallel to the NWs before and after annealing.

Figure 10 shows the XRD patterns of the as deposited $(Fe_{30}Co_{70})_{98}Zn_2$ and $(Fe_{30}Co_{70})_{95}Zn_5$ samples before annealing and after annealing at 575 °C. The annealing process does not have any significant effect on the crystal structure of the $(Fe_{30}Co_{70})_{98}Zn_2$ sample. Therefore, the improvement in Hc and Sq values of this sample is not related to microstructure change but can be mainly attributed to the release of stress in the crystal lattice. There is a high level of intrinsic stress and defects in the crystal structure of as prepared NWs due to the rapid electrodeposition of Fe, Co and Zn atoms into the template. Annealing at high temperature relieves the internal stress and defects in the NWs and slightly increases the Ms of annealed samples, thus improving the Hc and Sq values. On the other hand, for $(Fe_{30}Co_{70})_{95}Zn_5$ samples a (1 1 0) peak appears in the XRD pattern after annealing, indicating that this sample has bcc structure. The change in the magnetic properties of this sample before and after the annealing process can thus be attributed to significant changes in their microstructural properties.

4. Conclusion

Highly ordered NW arrays of $(Fe_{30}Co_{70})_{100-x}Zn_x$ ($x =$ 0, 1, 2, 5, 7.5, 10) with 37 nm in diameter and high aspect ratio were fabricated by co-electrodeposition of Fe, Co and Zn into pores of anodized aluminum oxide (AAO) templates. The effect of the Zn concentration in the electrolyte as well as annealing on the magnetic properties of the deposited NWs has been investigated. It was found that composition and annealing temperature influence the Hc and Sq of the NW arrays. Increas-

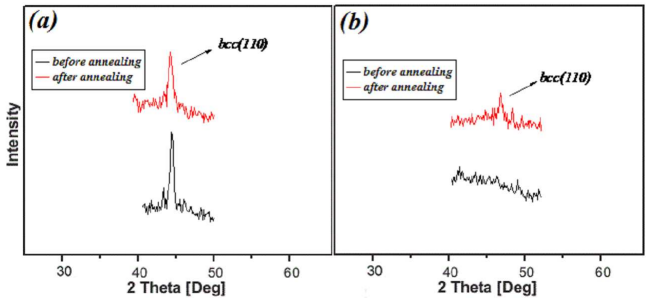

Fig. 10. The XRD patterns of the as deposited (a) $(Fe_{30}Co_{70})_{98}Zn_2$ and (b) $(Fe_{30}Co_{70})_{95}Zn_5$ samples before annealing and after annealing at 575 °C.

ing the Zn concentration in the electrolyte leads to a change in the crystal structure from the polycrystalline bcc structure of NWs to an amorphous phase, resulting in deterioration of both Hc and Sq. Magnetic properties of the samples were significantly improved by appropriate annealing process. After annealing the $(Fe_{30}Co_{70})_{98}Zn_2$ and $(Fe_{30}Co_{70})_{95}Zn_5$ samples showed the best magnetic properties with Sq = 0.99 and Hc = 2670 Oe, repectively. Annealing the $(Fe_{30}Co_{70})_{95}Zn_5$ NW sample leads to a change in crystal structure from amorphous phase to bcc structure with (1 1 0) texture along the NW axis.

References

[1] X.Y. Yuan, G.S. Wu, T. Xie, Y. Lin, L.D. Zhang, *Nanotechnology* **15**, 59 (2004).

[2] X.H. Bao, F.Y. Li, R.M. Metzger, *J. Appl. Phys.* **79**, 4866 (1996).

[3] M. Lederman, R. O'Barr, S. Schultz, *IEEE Trans. Magn.* **31**, 3793 (1995).

[4] A.J. Bennett, J.M. Xu, *Appl. Phys. Lett.* **82**, 3304 (2003).

[5] K. Nielsch, R.B. Wehrspohn, J. Barthel, J. Kirschner, U. Gosele, S.F. Fischer, H. Kronmuller, *Appl. Phys. Lett.* **79**, 1360 (2001).

[6] A. Blondel, J.P. Meier, B. Doudin, J.-P. Ansermet, *Appl. Phys. Lett.* **65**, 3019 (1994).

[7] O.K. Varghese, D.W. Gong, W.R. Dreschel, K.G. Ong, C.A. Grimes, *Sens. Actuators B* **94**, 27 (2003).

[8] F. Matsumoto, K. Nishio, H. Masuda, *Adv. Mater.* **16**, 2105 (2004).

[9] S. Ono, M. Saito, M. Ishiguro, H. Asoh, *J. Electrochem. Soc.* **151**, 473 (2004).

[10] J.R. Lim, J.F. Whitacre, J.P. Fleurial, C.K. Huang, M.A. Ryan, N.V. Myung, *Adv. Mater.* **17**, 1488 (2005).

[11] J. Choi, Y. Luo, R.B. Wehrspohn, R. Hillebrand, J. Schilling, U. Gosele, *J. Appl. Phys.* **94**, 4757 (2003).

[12] J. Li, C. Papadopoulos, J.M. Xu, M. Moskovits, *Appl. Phys. Lett.* **75**, 367 (1999).

[13] R. Fan, Y.Y. Wu, D.Y. Li, M. Yue, A. Majumdar, P.D. Yang, *J. Am. Chem. Soc.* **125**, 5254 (2003).

[14] T.M. Whitney, P.C. Searson, J.S. Jiang, C.L. Chien, *Science* **261**, 1316 (1993).

[15] H. Masuda, K. Fukuda, *Science* **268**, 1466 (1995).

[16] P.S. Fodor, G.M. Tsoi, L.E. Wenger, *J. Appl. Phys.* **91**, 8186 (2002).

[17] M.A. Kashi, A. Ramazani, F. Es'haghi, S. Ghanbari, A.S. Esmaeily, *Physica B* **405**, 2620 (2010).

[18] D.-H. Qin, Y. Peng, L. Cao, H.-L. Li, *Chem. Phys. Lett.* **374**, 661 (2003).

[19] S.L. Tang, W. Chen, M. Lu, S.G. Yang, F.M. Zhang, Y.W. Du, *Chem. Phys. Lett.* **384**, 1 (2004).

[20] Y.J. Bing, L.Z. Yi, C.W. Ming, D.K. Feng, Y.X. Fei, L.G. Qi, *Mater. Sci. Eng. B* **150**, 141 (2008).

[21] D.S. Xue, J.L. Fu, H.G. Shi, *J. Magn. Magn. Mater.* **308**, 1 (2007).

[22] J.L. Fu, Z.J. Yan, Y. Xu, X.L. Fan, D.S. Xue, *J. Phys. Chem. Solids* **68**, 2221 (2007).

[23] X.Y. Yuan, G.S. Wu, T. Xie, B.Y. Geng, Y. Lin, G.W. Meng, L.D. Zhang, *Solid State Sci.* **6**, 735 (2004).

[24] J. In, K.S.K. Varadwaj, K. Seo, S. Lee, Y. Jo, M.-H. Jung, J. Kim, B. Kim, *J. Phys. Chem. C* **112**, 4748 (2008).

[25] A.L. Schmitt, J.M. Higgins, S. Jin, *Nano Lett.* **8**, 810 (2008).

[26] R.L. Wang, S.L. Tang, Y.G. Shi, X.L. Fei, B. Nie, Y.W. Du, *J. Appl. Phys.* **103**, 07D507 (2008).

[27] A. Saedi, M. Ghorbani, *Mater. Chem. Phys.* **91**, 417 (2005).

[28] K. Shimizu, K. Kobayashi, G.E. Thompson, G.C. Wood, *Philos. Mag.* **66**, 643 (1992).

[29] I.S. Jacobs, C.P. Bean, *Phys. Rev.* **100**, 1060 (1955).

[30] Y. Xu, J.L. Fu, D.Q. Gao, D.S. Xue, *J. Alloys Comp.* **495**, 450 (2010).

[31] D.-H. Qin, L. Cao, Q.Y. Sun, Y. Huang, H.-L. Li, *Chem. Phys. Lett.* **358**, 484 (2002).